Cement and Concrete Research 109 (2018) 54–63

Contents lists available at ScienceDirect

Cement and Concrete Research

journal homepage: www.elsevier.com/locate/cemconres

Sulfuric acid resistance of one-part alkali-activated mortars

P. Sturm[a], G.J.G. Gluth[a,*], C. Jäger[b], H.J.H. Brouwers[c], H.-C. Kühne[a]

[a] Bundesanstalt für Materialforschung und -prüfung (BAM), Division 7.4 Technology of Construction Materials, Unter den Eichen 87, 12205 Berlin, Germany
[b] Bundesanstalt für Materialforschung und -prüfung (BAM), Division 1.3 Structure Analysis, Richard-Willstätter-Straße 11, 12489 Berlin, Germany
[c] Eindhoven University of Technology, Department of the Built Environment, P.O. Box 513, Vertigo 6.10, 5600 MB Eindhoven, The Netherlands

ARTICLE INFO

Keywords:
Alkali activated cement (D)
Durability (C)
Characterization (B)
Spectroscopy (B)
One-part geopolymers

ABSTRACT

One-part alkali-activated (geopolymer) mortars based on three different silica-rich starting materials and sodium aluminate, with and without ground granulated blast furnace slag (GGBFS) addition, were tested regarding sulfuric acid resistance according to DIN 19573:2016-03 (70 days at pH = 1). Corresponding pastes were characterized by XRD, SEM, chemical analysis, ^{29}Si MAS NMR and ^{1}H-^{29}Si CPMAS NMR after water storage and after acid exposure. The mortars exhibited a high resistance against sulfuric acid attack, with the best ones conforming to the requirements of DIN 19573:2016-03. The analytical results showed that this was due to precipitation of silica gel at the acid-mortar interface, which formed a mechanically stable layer that protected the subjacent mortar and thus inhibited further degradation. The addition of GGBFS decreased the acid resistance via formation of expansive calcium sulfate phases.

1. Introduction

The long-term chemical resistance of concrete structures is of major importance for sustainable economies; one aspect in this context is that cementitious materials with a high acid resistance are required in many different important infrastructures, either for construction or for repair. In particular, concretes and mortars with high sulfuric acid resistance are needed for the construction and the repair of sewer structures, in which biogenic sulfuric acid attack is the major degradation mechanism [1–4]; improved acid resistance is also required in agricultural structures and biogas plants [2,5,6]. Important progress has been achieved in this regard with materials based on Portland cement (OPC)/supplementary cementitious materials (SCM) blends or calcium aluminate cement (CAC) [3,7–11], but ever-increasing demand justifies the search for alternative, potentially more durable binder systems.

Low-calcium alkali-activated materials (geopolymers and mortars/concretes produced from these) have been repeatedly observed to exhibit high acid resistance [12–18], making them promising materials for applications in the aforementioned environments, though exceptions from this general trend, i.e. unsatisfactory or ambiguous results of acid resistance tests, have been reported too [12,19–21]. Different parameters of the mix-design have been found to influence the acid resistance of geopolymers. The alkali ion of the activator solution appears to affect the pore size distribution of the binder matrix, potassium leading to larger pore sizes and thus lower acid resistance than sodium [12]. The addition of nano-silica or microsilica modifies the particle size distribution of the dry binder, potentially increasing the packing density of the solid particles in the fresh paste and thus improving its microstructure after hardening; furthermore, it is a way to modify the chemical composition (increase the SiO_2 content) of the system [16,17]. The presence or absence of dissolved silicate in the activator solution influences the crystallinity of the reaction products, which can impact the chemical resistance too [12]. Apparently the most important parameter is the CaO content of the binder: During sulfuric acid or sulfate attack, calcium may precipitate as gypsum, thereby causing expansion and damage [14,16,21]; under some circumstances, however, gypsum appears to block pores, inhibiting further corrosion [22].

All the above-mentioned studies were conducted on conventionally produced alkali-activated materials (AAMs), i.e. materials that were produced by addition of an alkali hydroxide or alkali silicate solution to a solid aluminosilicate powder. However, AAMs that need only to be mixed with water to initiate hardening (termed 'one-part mix' AAMs [23,24]) provide significant advantages regarding transport and storage of feedstocks, occupational health and safety, and adaption to conventional mixing and processing equipment, thus providing potentially a higher commercial viability. Different routes to precursors for one-part AAMs have been devised, including calcination or intense grinding of aluminosilicate materials together with alkali-bearing compounds, and dry mixing of (alumino)silicate materials with readily soluble solid activators [23–26].

One of these approaches is to dry-mix a silica-rich starting material and solid sodium aluminate ($NaAlO_2$), and subsequent mixing with

* Corresponding author.
E-mail address: gregor.gluth@bam.de (G.J.G. Gluth).

https://doi.org/10.1016/j.cemconres.2018.04.009
Received 27 February 2018; Received in revised form 9 April 2018; Accepted 10 April 2018

water [23,25]. In this approach, the properties and the phase assemblage after curing depend strongly on the employed silica material and the starting SiO_2/Al_2O_3 ratio, leading either to geopolymer-zeolite composites or to virtually fully amorphous geopolymers [27–29]. Besides the fact that the use of an alkaline solution for activation is avoided here, advantages of these binder systems include easy control of the SiO_2/Al_2O_3 ratio in a wide range as well as the possibility to use various industrial and biogenic by-products as silica-rich starting materials.

To the authors' knowledge, no previous studies of the acid resistance of one-part AAMs are available. In the present study, mortars were made with these binders, based on three different silica starting materials, with and without addition of ground granulated blast furnace slag (GGBFS). The mortars were tested for sulfuric acid resistance according to DIN 19573:2016-03 (70 days at pH = 1), and their binder microstructure characterized, using XRD, ^{29}Si MAS NMR, ^{1}H-^{29}Si CPMAS NMR, and SEM with regard to the mechanisms that are responsible for the observed acid resistance.

2. Materials and methods

2.1. Starting materials

Three different silica materials were employed as feedstocks: a microsilica (hereafter referred to as MS), a silica resulting from thermal treatment of residues from chlorosilane production and subsequent scrubbing and neutralization of the flue gas (CR), and a rice husk ash (RHA). The employed solid activator was sodium aluminate (nominally $NaAlO_2$). GGBFS was added to some formulations as a source of calcium. Chemical analysis of the solid feedstocks was performed by inductively coupled plasma optical emission spectrometry (ICP-OES) after total microwave digestion; the results are shown in Table 1. MS and RHA contained ~94 wt% SiO_2, while the SiO_2 content of CR was considerably lower (~84 wt%); RHA contained significant amounts of K_2O and P_2O_5. The sodium aluminate had an almost stoichiometric Na/Al ratio of 1.003 mol/mol.

The XRD patterns (Fig. 1; for measurement conditions see Section 2.4) showed a major hump with its maximum around 21.5° 2θ for CR and MS, evidencing a virtually fully amorphous silica with only minor crystalline impurities quartz (PDF # 00-046-1045), calcite (PDF # 01-086-0174) in CR, and residues of silicon (PDF # 00-027-1402) and silicon carbide (PDF # 00-049-1429) in MS. RHA contained, besides amorphous phase, a considerable amount of cristobalite (PDF # 00-039-1425) and minor amounts of tridymite (PDF # 00-042-1401). In a previous study on one-part AAMs [28], a fully amorphous rice husk ash was employed; the presence of cristobalite in the RHA used in the present work indicates a higher calcination temperature for the rice husks, probably above 800 °C [30]. The sodium aluminate consisted almost completely of anhydrous $NaAlO_2$ (PDF # 00-033-1200), and contained only minor amounts of hydrated sodium aluminates and natrite [27]. The GGBFS was almost fully amorphous (diffraction maximum at ~30.6° 2θ), and included minor amounts of merwinite ($Ca_3Mg(SiO_4)_2$; PDF # 00-035-0591).

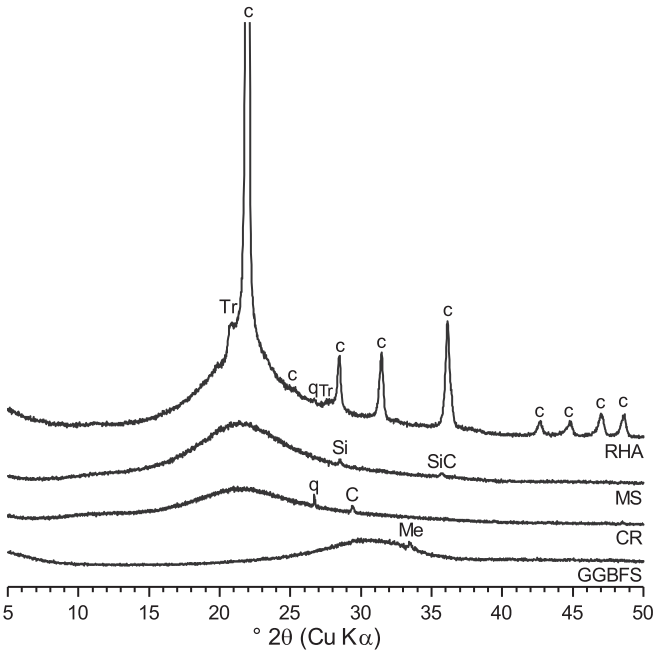

Fig. 1. XRD patterns of the starting materials RHA, MS, CR, and GGBFS (q = quartz; Tr = tridymite; c = cristobalite; C = calcite; Si = silicon; SiC = silicon carbide; Me = merwinite).

MS consisted of spherical primary particles with a diameter of approx. 50–200 nm, fused together to form larger agglomerates, as is typical for microsilicas. As seen in SEM micrographs [25], silica CR had a very similar particle morphology. The RHA exhibited angular particle shapes, and rough particle surfaces with many pore openings with sizes up to ~500 nm. The specific surface areas of the silica materials were determined by N_2 sorption at 77 K, employing the BET method for data evaluation, to be 20.1 m^2/g for MS, 32.3 m^2/g for CR, and 13.9 m^2/g for the RHA. The medium particle size, d_{50}, determined by laser granulometry, was 24.1 µm for RHA and 17.3 µm for the sodium aluminate.

CEN Standard sand (quartz; max. grain size: 2 mm) in accordance with DIN EN 196-1:2016-11 was used as aggregate for all mortars.

Table 1
Chemical composition of the starting materials.

Oxide	MS (wt%)	CR (wt%)	RHA (wt %)	Sodium aluminate (wt%)	GGBFS (wt %)
SiO_2	94.57	84.23	93.72	1.07	35.10
Al_2O_3	0.17	4.18	0.05	60.89	11.03
Fe_2O_3	0.04	0.43	0.10	0.02	0.42
TiO_2	0.01	0.06	0.01	< 0.01	< 0.01
CaO	1.15	2.97	0.97	0.52	40.64
MgO	0.23	0.17	0.38	0.01	8.26
Na_2O	0.14	0.22	0.26	36.78	0.55
K_2O	0.71	0.03	1.33	0.56	0.49
SO_3	0.21	0.16	0.35	0.08	2.20
P_2O_5	0.14	-	0.63	-	-
LOI	1.84	5.08	1.74	1.00	1.05
CO_2	-	4.20	-	0.03	0.36
Residual	0.82	2.51	0.49	0.16	0.29

LOI: loss on ignition (1000 °C); includes CO_2.
-: not determined.

2.2. Sample preparation

Table 2 gives the compositions of the investigated mortars in terms of the molar SiO_2/Al_2O_3 ratio of the binder, the water/binder weight

Table 2
Mix-designs of the one-part alkali-activated mortars.

Sample designation	SiO_2/Al_2O_3 (mol/mol)	w/b (g/g)	Paste content (wt%)	Na_2O/CaO (mol/mol)	H_2O/(Na_2O + CaO) (mol/mol)
MS_6	6.03	0.40	31.5	10.66	11.44
MS_6_b	6.03	0.40	37.4	10.66	11.44
MS_6_SL	6.31	0.38	30.0	0.80	6.74
RHA_6_b	6.05	0.40	37.6	12.40	11.30
RHA_6_SL_b	6.38	0.38	38.2	0.80	6.67
CR_3.5	3.52	0.50	30.7	6.36	11.10

ratio (w/b), the paste content by weight (remainder: aggregates), and the molar Na_2O/CaO ratio of the binder. The SiO_2/Al_2O_3 ratio was defined by the relative proportions of the silica material and the sodium aluminate in the dry binder; the Na_2O/CaO ratio was determined by the amount of CaO in the silica materials and the addition of GGBFS; and the $H_2O/(Na_2O + CaO)$ was determined by the w/b. The actual $H_2O/(Na_2O + CaO)$ ratios determines the hydration of dissolved Na^+ and Ca^{2+} ions in the pore solution and influences its pH and viscosity; its total value (and thus hypothetical minimum) is given in Table 2 for comparison purposes. In the sample designations, MS/RHA/CR denote the employed silica material, the subsequent number gives the approximate SiO_2/Al_2O_3 ratio, SL denotes the addition of GGBFS, and the letter b is used to denote mortars with increased paste content (~38 wt% instead of ~31 wt%).

The mortars with GGBFS had a total CaO content of the dry binder of 10 wt% (i.e. ~25 wt% GGBFS). The finite Na_2O/CaO ratios of the mortars without GGBFS were caused by the minor CaO contents of the silica starting materials (Table 1). Mortar CR_3.5 had to be produced with a lower SiO_2/Al_2O_3 ratio and a higher w/b than the other mortars due to insufficient workability at the mix-design chosen for the other mortars.

Mixing of the mortars was done in a standard mortar mixer according to DIN EN 196-1:2016-11. The fresh mortars were cast in two layers into 40 mm × 40 mm × 160 mm prism molds and each layer compacted by vibrating the molds. Curing was done in a climate chamber at 60 °C (GGBFS-containing mortars) or 80 °C (mortars without GGBFS) and 80% relative humidity (RH) for 24 h. Subsequently, the mortar prisms were removed from the molds and prepared for sulfuric acid resistance testing as described in Section 2.3. The different curing temperatures for the mortars with and without GGBFS were chosen based on preliminary experiments which showed that curing the GGBFS-containing mortars at temperatures above 60 °C does not lead to improved performance in terms of strength development, while optimum strength for the mortars without GGBFS were achieved at 80 °C.

In addition to the mortars for sulfuric acid resistance testing, paste samples were prepared for microstructural analyses. The pastes had the same composition as the pastes of the corresponding mortars with the same sample designation. The pastes were mixed in a planetary centrifugal mixer at a rotation speed of 1100 min^{-1} for a total of 9 min with a short break after every 3 min to allow the mixer to cool (RHA-based pastes) or at 1200 min^{-1} for 3 min (MS-based pastes). Subsequently, the pastes were cast into 20 mm × 20 mm × 20 mm silicone cube molds. Curing was done as for the mortar specimens. No bleeding or segregation of the pastes was observed by visual inspection, which was most likely caused by the comparatively high specific surface area of the silica starting materials.

Subsequently, the paste cubes were stored, soaked in water, and exposed to either sulfuric acid or water exactly as the mortar specimens (Section 2.3) up to the time of removal from the acid bath. The GGBFS-free pastes remained in the acid bath together with the corresponding mortars for the full time of the test (70 days). The GGBFS-containing pastes started to disintegrate after approx. 14 days. Therefore, they were transferred to 400-ml beakers and immersed in sulfuric acid (pH = 1) for the remainder of the test time; the acid solution was replaced with fresh solution once a week.

After the acid or water treatment, the paste samples were rinsed with deionized water and dried in an oven at 40 °C for 1 day. Subsequently, the samples were either crushed for SEM investigations or ground manually using mortar and pestle (agate), until all particles passed through a sieve with 0.063-mm mesh width. The samples were stored in a desiccator above dry silica gel until required for analyses.

2.3. Sulfuric acid resistance testing

The acid resistance of the mortars was determined in accordance with the German standard DIN 19573:2016-03 'Mortar for construction and rehabilitation of drains and sewers outside buildings', Appendix A, except adjustments regarding the curing regime of the mortars. Currently, the standard is only available in German, therefore, we provide a detailed description here.

For each sample series, five mortar prisms were prepared as described in Section 2.2. After removal from the molds, the surfaces of the prisms were ground manually for 15 s with abrasive paper (graining 320) to remove the outer paste layer. Subsequently, the specimens were further cured at 23 °C and 50% RH for 25 days. At an age of 7 days, the mortar prisms were cut into halves (40 mm × 40 mm × 80 mm), and their dimension were measured precisely. At an age of 26 days, all specimens were immersed in tap water at 23 °C for 2 days to saturate their (outer) pores. After the total curing time of 28 days, half of the specimens were transferred to a sulfuric acid (H_2SO_4 solution; pH = 1) bath, and the other samples remained under water. The specimens in the sulfuric acid bath were immersed at least 10 mm below the surface in a volume of ≥ 8 dm^3 of sulfuric acid. The cut mortar prisms were placed on grates, and the solution constantly stirred by a magnetic stirrer to ensure homogeneous exposure to the acid. An automatic titration system was used to keep the pH at 1, and the consumed amount of acid was recorded. In addition, the test solution was replaced with new acid once per week.

After 70 days of exposure to the sulfuric acid or water (sample age 98 days), the specimens were removed from the respective tanks, loose material was removed from their surfaces with a soft brush, and the new specimen dimensions were determined. The mortar specimens were then cut and ground to a height of 40 mm. After subsequent storage at 23 °C and 50% RH for 2 days, the mortar specimens were tested for compressive strength according to DIN EN 196-1:2016-11 (compression parallel to the principal axis of the original prisms). Table 3 summarizes the curing and the acid or water exposure conditions and lengths.

From the fracture loads of the acid-immersed and the water-immersed samples, the relative residual compressive strength, f_{rel} (symbol not used in DIN 19573:2016-03), and the effective depth of corrosion, $X_{f,D}$, were calculated according to:

$$f_{rel} = \frac{F_{D,acid}/(40\ mm \times 40\ mm)}{F_{D,water}/(a \times b)} \times 100\% \quad (1)$$

$$X_{f,D} = 0.5 \times d_0 \times \left[1 - \sqrt{\frac{F_{D,acid}}{F_{D,water}}}\right] \quad (2)$$

Table 3
Curing and testing conditions for the one-part alkali-activated mortars and pastes (uW = under water storage; REF = reference, i.e. water exposure).

Sample	Curing: 28 days			H_2SO_4 or REF: 70 days	Drying: 2 days
MS_6	1 day @ 80 °C/80% RH	25 days @ 23 °C/50% RH	2 days @ 23 °C/uW	70 days @ 23 °C/pH = 1 or 70 days @ 23 °C/uW	2 days @ 23 °C/50% RH
MS_6_b	1 day @ 80 °C/80% RH				
MS_6_SL	1 day @ 60 °C/80% RH				
RHA_6_b	1 day @ 80 °C/80% RH				
RHA_6_SL_b	1 day @ 60 °C/80% RH				
CR_3.5	1 day @ 80 °C/80% RH				

$$d_0 = \sqrt{(a \times b)} \quad (3)$$

where $F_{D,acid}$ and $F_{D,water}$ are the fracture loads of the acid-immersed and the water-immersed samples, respectively, and a and b are the edge lengths of the tested cross-sections of the water-immersed specimens. The use of 40 mm × 40 mm in the numerator, but $a \times b$ in the denominator of Eq. (1) is prescribed in the standard; the introduced error is however minor, as the edge lengths a and b of the water-immersed specimens will generally be approx. 40 mm.

The requirements for sulfuric acid resistance (pH = 1) specified in DIN 19573:2016-03 are: $f_{rel} > 75\%$, and $X_{f,D} < 2.7$ mm; these two requirements are equivalent (Eqs. (1) and (2)). The effective depth of corrosion corresponds to the hypothetical depth of corrosion, caused by the exposure to sulfuric acid, that would be observed if the compressive strength of the unaffected core was equal to the compressive strength of the water-immersed specimen, and the strength of the corroded layer was zero.

In the discussion below, the compressive strength of the specimens after 70-day water-immersion will be referred to; it will be denoted reference strength, $f_{D,water}$, and is defined as:

$$f_{D,water} = \frac{F_{D,water}}{a \times b} \quad (4)$$

2.4. Microstructural analyses

X-ray diffraction (XRD) patterns were recorded on a Rigaku Ultima IV diffractometer in Bragg-Brentano geometry under the following conditions: Cu Kα radiation (λ = 1.5419 Å), 40 kV, 40 mA; divergence slit: 10 mm in-plane, 0.5° axial; sampling interval = 0.02° 2θ; scan rate = 0.5° 2θ min^{-1}; scanning range: 5–65° 2θ; strip detector D/teX Ultra. Samples were rotated at a speed of 15 min^{-1} during the measurements.

^{29}Si magic-angle spinning nuclear magnetic resonance (MAS NMR) single-pulse spectra were recorded on a Bruker AVANCE 600 spectrometer at 119.2 MHz, using a 4-mm triple-resonance probe with a sample spinning speed of 12.5 kHz. All spectra were recorded at room temperature with a 90° pulse of 6 μs, and at least 24 scans were accumulated per specimen. The recycle delay was set to 900 s because of observed long relaxation times for some of the present species (cf. Ref. [27]). ^{1}H-^{29}Si CPMAS NMR spectra were collected on the same spectrometer with a contact pulse length of 2 ms and a recycle delay of 3 s, accumulating at least 512 scans per spectrum. Chemical shifts were referenced using kaolinite as a secondary standard with −91.5 ppm for its upfield peak. The $Q^n(m\text{Al})$ nomenclature for SiO_4 tetrahedra will be used throughout this article, where n denotes number of oxygen-bridges to neighboring SiO_4 and AlO_4 tetrahedra, and $m \leq n$ denotes the number of AlO_4 of these tetrahedra; for $m = 0$, the expression in parentheses is omitted.

Scanning electron microscopy (SEM) investigations were performed on a Carl Zeiss EVO MA10 device at an accelerating voltage of 7–10 kV in secondary electron (SE) mode. Samples were sputtered with gold before the measurements.

3. Results and discussion

3.1. Mortar strength and acid resistance

The results of the sulfuric acid resistance tests of the mortars are shown in Table 4. Mortar MS_6 had a relative residual compressive strength (f_{rel}) of 72%, and an effective depth of corrosion ($X_{f,D}$) of 3.1 mm; this is close to the requirements of DIN 19573:2016-03. For mortar MS_6_b, with the same paste composition but an increased paste content compared to MS_6, the measured values were f_{rel} = 77.1% and $X_{f,D}$ = 2.5 mm, conforming to the requirements of DIN 19573:2016-03 for mortars to be used in sewer repair. The reference strength, $f_{D,water}$, of mortar MS_6_b was lower than $f_{D,water}$ of MS_6, which is attributed to the higher paste content of MS_6_b.

Table 4
Compressive strength after storage for 70 days in water ($f_{D,water}$), relative residual compressive strength (f_{rel}) and effective depth of corrosion ($X_{f,D}$) of the mortars. Values after the plus/minus sign denote standard deviations. Bold entries denote values that conform to the requirements of DIN 19573:2016-03.

Sample	$f_{D,water}$ (MPa)	f_{rel} (%)	$X_{f,D}$ (mm)
MS_6	58.0 ± 4.5	72.0	3.1
MS_6_b	41.0 ± 0.8	**77.1**	**2.5**
MS_6_SL	53.6 ± 5.3	62.5	4.2
RHA_6_b	32.0 ± 4.1	**77.9**	**2.4**
RHA_6_SL_b	30.3 ± 1.3	57.2	5.0
CR_3.5	48.7 ± 0.7	52.9	5.6

The relative residual compressive strength of mortar RHA_6_b after the acid treatment was 77.9%, which was almost equal to that of the similarly composed mix MS_6_b. However, its reference strength was lower than that of MS_6_b, indicating a generally slower hardening for the RHA. This is in contrast to previous studies, in which it was found that geopolymer pastes produced from another rice husk ash had considerably higher strengths than geopolymer-zeolite composite pastes based on MS [27,28]. This difference is attributed to the higher fraction of inert crystalline impurities (mainly cristobalite) of the RHA used in the present study, which will cause a lower overall reactivity, and possibly also to a tendency of the MS-based binder to bond better to the aggregates of the mortar.

Mortar CR_3.5 exhibited significantly lower resistance to sulfuric acid attack than the other mortars: The relative residual compressive strength of the acid-exposed specimens was only 52.9%, and the effective depth of corrosion, $X_{f,D}$, was 5.6 mm. These values were the lowest f_{rel} and the highest $X_{f,D}$, respectively, of all considered mortars. This is mainly related to the significantly higher w/b of mortar CR_3.5 as compared to the other mortars, which is expected to cause a higher porosity and thus much easier ingress of the sulfuric acid.

The mortars with GGBFS addition generally performed worse than the analogous mortars without slag addition in the acid resistance tests (Table 4). MS_6_SL possessed a f_{rel} of 62.5% and a $X_{f,D}$ of 4.2 mm, and RHA_6_SL_b had f_{rel} = 57.2% and $X_{f,D}$ = 5.0 mm. It was observed that the mortars with GGBFS addition underwent slight expansion during the acid treatment, in contrast to the mortars without CaO addition. Crack formation related to this expansion is considered to be the main reason for their lower sulfuric acid resistance, as is discussed in more detail in Sections 3.2 and 3.4.

Cross-sections of cut mortars specimens after acid exposure, sprayed with phenolphthalein solution, are shown in Fig. 2. All specimens exhibited an apparently unaffected core, and a corroded outer layer. The color of the cores in Fig. 2 differed mainly due to the fact that the wettability of the surfaces differed between specimens, the wettability of the RHA-based mortars being generally better compared to the other mortars. The reason for this behavior may be the porous nature of unreacted RHA (Sections 3.2 and 3.3) in the mortars. However, a different degree of leaching of alkalis towards the exterior is probably also partly responsible for the observed differences.

Notably, for the GGBFS-free mortars, only a thin layer of material was lost during cleaning the specimens after acid exposure with a brush, and the remaining corroded layer did not spall or disintegrate, and retained some mechanical strength. In these mortars, the depth of the corroded layer that could be visually observed with the naked eye corresponded roughly to the calculated effective depth of corrosion, $X_{f,D}$. The GGBFS-containing mortars exhibited somewhat more loss of material after brushing, as is apparent from the rounded corners of these mortars in Fig. 2. However, also with the GGBFS-containing mortars, the main part of the corroded layer did not disintegrate, and it retained some mechanical strength. These observations regarding the

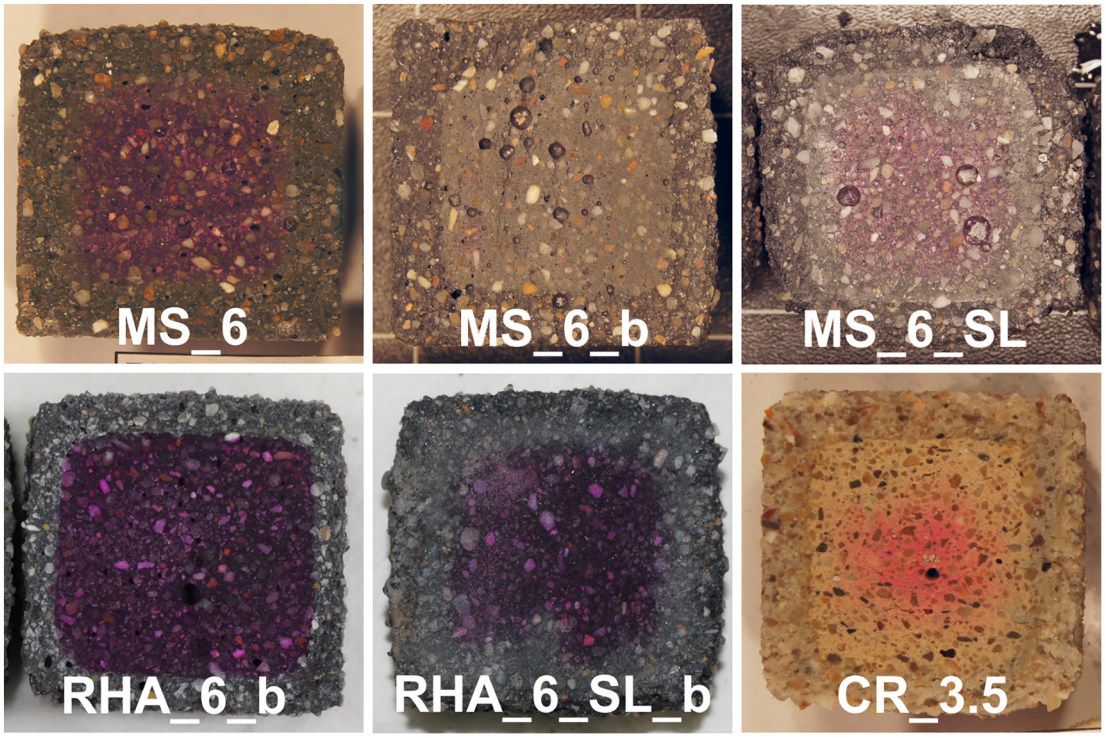

Fig. 2. Cross-sections, sprayed with phenolphthalein solution, of the mortars MS_6, MS_6_b, and MS_6_SL (top row, from left to right), and RHA_6_b, RHA_6_SL_b, and CR_3.5 (bottom row, from left to right) after the 70-day exposure to sulfuric acid (pH = 1). (For interpretation of the references to color in this figure, the reader is referred to the web version of this article.)

visual appearance of the cross-sections were in general agreement with the relative order of the acid resistance (f_{rel} and $X_{f,D}$) of the mortars.

3.2. XRD analyses

To elucidate the processes that determine the observed acid resistance of the mortars, selected paste specimens, with the compositions of the corresponding mortars, were subjected to microstructural analyses; the omittance of the quartz aggregates in these samples facilitated easier identification of changes that occurred in the binder phase. As the visually observed corrosion depth and the effective depth of corrosion, $X_{f,D}$, of the mortars were on the order of 2.5 to 6 mm, and the paste samples lacked the quartz aggregate that is inert and thus hinders ingress of the acid by increasing the tortuosity of the diffusion paths, it can be assumed that the paste samples that were exposed to the sulfuric acid for 70 days were fully corroded. Visual inspection of split paste samples revealed a homogeneous appearance, i.e. an unaffected core could not be identified, indicating that the above assumption was satisfied.

Figs. 3 to 6 show the XRD patterns of the pastes MS_6, MS_6_SL, RHA_6_b, and RHA_6_SL_b, respectively, after 70-day water-immersion and after 70 day exposure to the sulfuric acid, as well as the respective starting silica for comparison. In all cases, the XRD patterns after the 70-day water-immersion were virtually identical to XRD patterns of the as-cured pastes (not shown), confirming that the immersion of the pastes in water did not induce any significant phase transformations or dissolution.

The diffractogram of paste MS_6 (Fig. 3) after water-immersion exhibited major reflections of zeolite A ($Na_4(AlSiO_4)_4{\cdot}9H_2O$; PDF # 00-039-0222) and minor amounts of hydrosodalite ($Na_6(AlSiO_4)_6{\cdot}4H_2O$; PDF # 00-042-0216), as well as an amorphous hump that is broadened towards higher diffraction angles, compared to the starting silica MS. The persistence of a hump with a maximum at ~22° 2θ is attributed to remaining (unreacted) silica MS in the material, while the asymmetric broadening towards ~29° 2θ is caused by geopolymeric gel that has

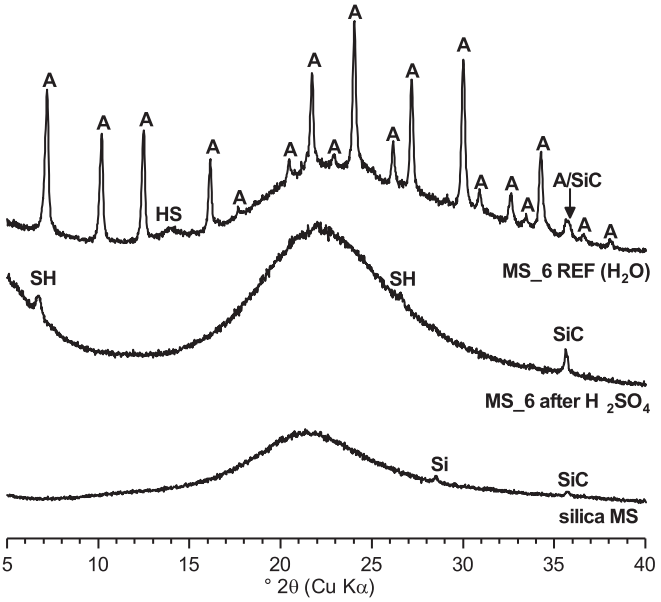

Fig. 3. XRD patterns of paste MS_6 after 70-day water-immersion and after 70-day exposure to sulfuric acid (pH = 1), and of the silica MS (A = zeolite A; HS = hydrosodalite; Si = silicon; SiC = silicon carbide; SH = silicic acid).

precipitated during hardening. In addition, the silicon carbide impurity of the silica feedstock remained visible in the diffractogram of the paste. These results are in agreement with the phase assemblage for as-cured pastes with the same composition, reported in a previous study [27].

The XRD pattern of MS_6 after exposure to sulfuric acid exhibited a dominant, broad hump with its maximum at ~22° 2θ and minor peaks of silicic acid ($H_2Si_{14}O_{29}{\cdot}nH_2O$; PDF # 00-045-0423), while reflections of zeolite A, hydrosodalite, and the geopolymeric gel were absent. No

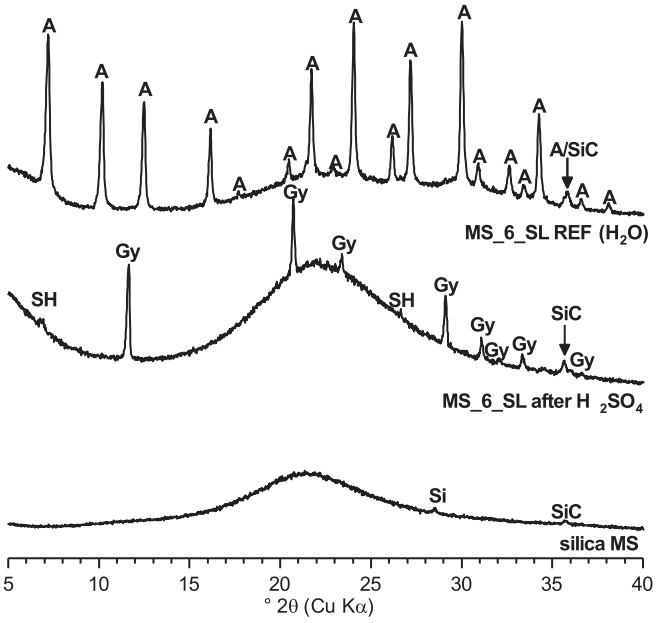

Fig. 4. XRD patterns of paste MS_6_SL after 70-day water-immersion and after 70-day exposure to sulfuric acid (pH = 1), and of the silica MS (A = zeolite A; Si = silicon; SiC = silicon carbide; SH = silicic acid; Gy = gypsum).

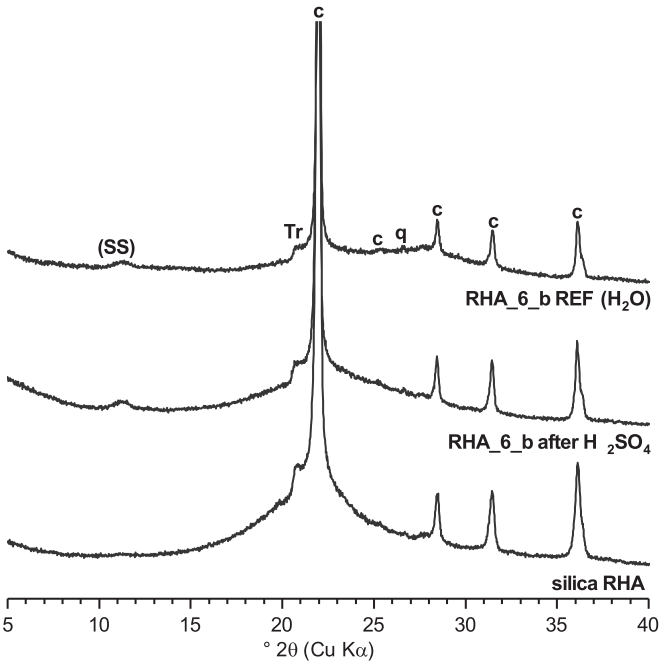

Fig. 5. XRD patterns of paste RHA_6_b after 70-day water-immersion and after 70-day exposure to sulfuric acid (pH = 1), and of the silica RHA (q = quartz; Tr = tridymite; c = cristobalite; (SS) = sodium silicate (uncertain)).

sulfates were identified in the diffractogram. These results show that the zeolites as well as the geopolymeric gel were dissolved in the sulfuric acid, while a silica material remained in place.

The GGBFS-containing paste MS_6_SL (Fig. 4) exhibited similar XRD patterns after water-immersion as the GGBFS-free MS_6. Zeolite A was the major crystalline phase (while hydrosodalite was missing), and a broad amorphous hump indicated the presence of unreacted silica and geopolymeric gel. However, the more pronounced hump around ~29° 2θ, compared to MS_6, indicated a higher degree of reaction of the silica and higher fraction of geopolymeric gel in MS_6_SL. Indications of calcium aluminosilicate hydrate (C-A-S-H) would be difficult to detect

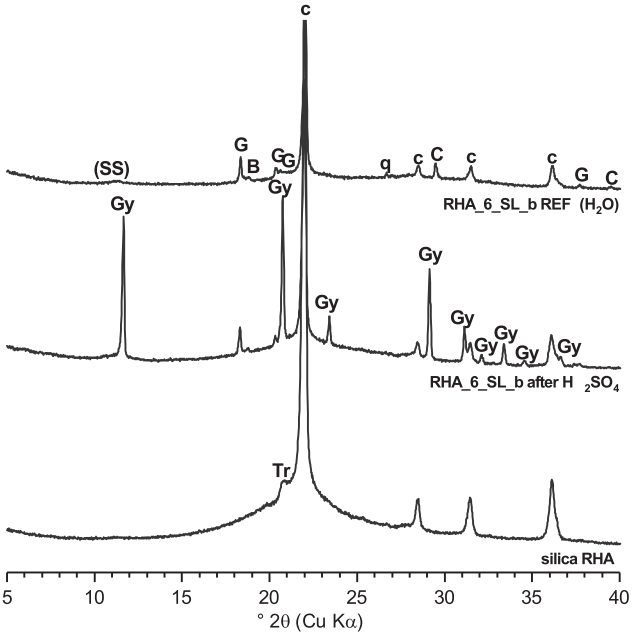

Fig. 6. XRD patterns of paste RHA_6_SL_b after 70-day water-immersion and after 70-day exposure to sulfuric acid (pH = 1), and of the silica RHA (q = quartz; Tr = tridymite; c = cristobalite; (SS) = sodium silicate (uncertain); g = gibbsite; B = bayerite; C = calcite; Gy = gypsum).

in the XRD patterns, and thus its formation cannot be ruled out from these measurements. However, Ismael et al. [31] found that for fly ash/GGBFS-based AAMs, geopolymeric gel ('N-A-S-H gel') is the only binder phase for GGBFS contents ≤ 25 wt% (i.e. CaO contents below ~10 wt %), though the geopolymeric gel may be partly modified by the incorporation of Ca. Since no indications of C-A-S-H gel were found in the XRD pattern and, more importantly, also not in the ^{29}Si MAS NMR spectra (Section 3.3), it is concluded that this is valid for the present MS-based one-part AAMs too.

After the acid exposure of MS_6_SL, a broad amorphous hump, centered at ~22° 2θ, and reflections of significant amounts of gypsum (PDF # 00-033-0311) as well as small amounts of silicic acid were present in the diffractogram. That means, that, similar to what was observed for MS_6, all zeolites and the geopolymeric gel had dissolved, but in addition the sulfuric acid attack induced precipitation of gypsum. This is attributed to the increased CaO content of MS_6_SL, viz. calcium reacted with the sulfate anion to precipitate as hydrated calcium sulfate. Gypsum formation caused by sulfuric acid attack on AAMs with significant CaO content has been observed earlier and related to expansion and cracking of the materials [14,16,21]. In the present study too, the relation between gypsum formation and expansion and related cracking is obvious, and is considered to be the main reason for the lower sulfuric acid resistance of the GGBFS-containing mixes.

The XRD pattern of paste RHA_6_b after water-immersion (Fig. 5) differs from the diffractogram of MS_6 in that no zeolites are present. Instead, the diffractogram contains reflections of the crystalline phases of the RHA feedstock (cristobalite and tridymite), a prominent hump around 29° 2θ, and a small feature at low diffraction angles that may be related to poorly crystalline sodium silicate (cf. PDF # 00-027-0709). These results are broadly in line with previous results [28] that demonstrated that one-part AAMs based on a mix of fully amorphous rice husk ash and sodium aluminate (starting SiO_2/Al_2O_3 = 3.5) lead to a fully amorphous geopolymer with no crystalline by-products and a near-to-complete reaction of the rice husk ash. Deviating from the results for the high-reactivity rice husk ash, RHA_6_b contained non-reactive crystalline phases of the RHA and possibly some sodium silicate that had formed from excess sodium and silicate.

After acid exposure, the hump around 29° 2θ had disappeared from the diffractogram, at least partly, indicating dissolution of the geopolymer. No sulfate phases were present, and the diffractogram indicated the presence of a silica phase, superimposed by the base of the major cristobalite peak at 22° 2θ.

The diffractogram of the GGBFS-containing paste RHA_6_SL_b after water-immersion (Fig. 6) demonstrated the presence of gibbsite (PDF # 00-033-0018) as well as minor amounts of bayerite (PDF # 00-020-0011) and calcite (PDF # 01-086-0174). A hump around 29° 2θ was present, indicating the formation of geopolymeric gel, as for RHA_6_b. Analogous to the above discussion for MS_6_SL, it can be assumed that precipitation of large amounts of C-A-S-H has not been taken place in RHA_6_SL_b. However, the ^{29}Si MAS NMR results (Section 3.3.) suggest, that in RHA_6_SL_b a small amount of C-A-S-H had formed.

The XRD pattern of RHA_6_SL_b after exposure to sulfuric acid exhibited major reflections of gypsum, while the geopolymer had largely dissolved. As for RHA_6_b, the diffractogram indicated the presence of a silica phase, superimposed by the base of the major cristobalite peak.

3.3. NMR analyses

Fig. 7 shows the single-pulse ^{29}Si MAS NMR spectra of the MS-based pastes after water-immersion and after acid-exposure for 70 days. For the water-immersed pastes, three major resonances at around −110 ppm, −98 ppm, and −89 ppm are observed, as well as a shoulder at approx. −85 ppm, which is more marked for MS_6. These features have been assigned previously [27,29] to Q^4 species of unreacted silica at −110 ppm, Q^3 species in the hydrated outer layer of the unreacted silica at −98 ppm, Q^4(4Al) species in zeolite A at approx. −89 ppm, and Q^4(4Al) species of a low-Si ($SiO_2/Al_2O_3 \approx 2$) geopolymeric gel centered at −85 ppm.

The intensity of the Q^4 and Q^3 resonances relative to the intensity of Q^4(4Al) resonance is significantly lower for MS_6_SL than for MS_6, confirming that the degree of reaction of the silica MS was higher in MS_6_SL, as deduced above from the XRD results. Indications of C-A-S-H gel, viz. Q^1 around −79 ppm, Q^2 or Q^2(1Al) at –(86…80) ppm, and low amounts of Q^3(1Al) at −(94…89) ppm [32–34], cannot be identified in the spectrum of MS_6_SL, in accord with the above statement that no C-A-S-H was formed (though it cannot be fully excluded that minor amounts of these species may be superimposed by the resonances of the Q^4(4Al) species of the geopolymeric gel in the spectrum). Further, a significant amount of unreacted GGBFS, that would be visible by its Q^0 species at −74 ppm [34], cannot be distinguished in the spectrum of MS_6_SL; it can thus be concluded that the GGBFS has reacted virtually completely.

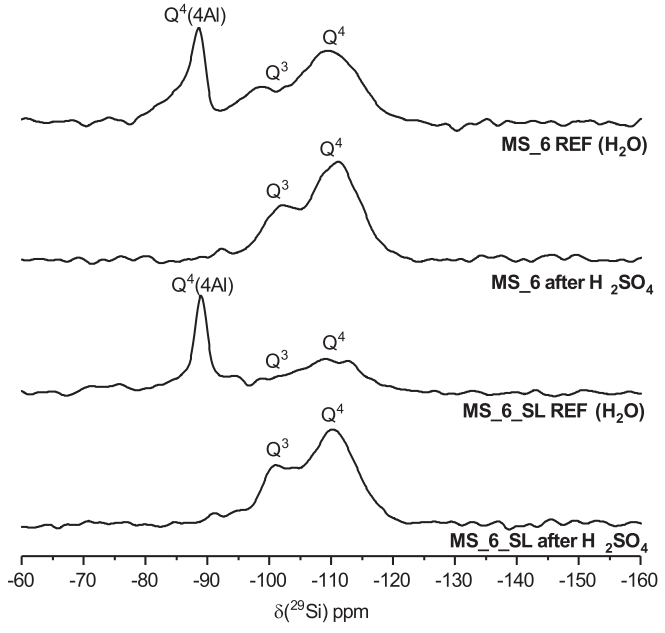

Fig. 7. ^{29}Si MAS NMR single-pulse spectra of the pastes MS_6 and MS_6_SL after 70-day water-immersion and after 70-day exposure to sulfuric acid (pH = 1).

For both, MS_6 and MS_6_SL, exposure to sulfuric acid led to almost complete disappearance of the resonances of the Q^4(4Al) species from the spectrum, leaving only Q^4 and Q^3 species. The assignment of the resonance around −98 ppm to Al-free Q^3 species is supported by a chemical analysis of paste MS_6 after the 70-day sulfuric acid exposure (done as for the starting materials, Section 2.1, i.e. by ICP-OES after total microwave digestion), that gave 84.62 wt% SiO_2, 1.13 wt% Al_2O_3, 0.54 wt% CaO, 0.62 wt% Na_2O, 0.72 wt% SO_3, and 11.03 wt% LOI, showing that Al was almost absent in the specimen. The results prove that the zeolites and the geopolymeric gel had dissolved during the acid attack, and silica phase(s) remained and/or was newly formed. The latter will be discussed in more detail below in connection with the ^{1}H-^{29}Si CPMAS NMR spectra of the acid-exposed, RHA-based pastes.

The ^{29}Si MAS NMR single-pulse and the ^{1}H-^{29}Si CPMAS NMR spectra of RHA_6_b after water-immersion are shown in Fig. 8 (top two spectra). The single-pulse spectrum exhibits a sharp peak at −109 ppm on top of a broader resonance centered around the same value, a broad feature around −99 ppm, and a large shoulder extending to approx. −80 ppm (gray bar in Fig. 8). The narrow peak at −109 ppm is attributed to the unreacted cristobalite in the material [35,36]. The broad resonances around −109 ppm and − 99 ppm can be assigned analogously to the resonances in the spectra of MS_6 and MS_6_SL to unreacted (amorphous) silica and its hydrated surface layer, respectively. The broad feature, extending from near the Q^3 resonance (−99 ppm) to about −80 ppm indicates the presence of different Q^4(mAl) species with m ranging from 1 to 4, which is the distinguishing feature of 'optimum' geopolymers with a molar SiO_2/Al_2O_3 ratio around 3.5 to 4 [37–40], in line with the XRD results above. In the CPMAS spectrum of RHA_6_b after water-immersion, the resonance of the Q^4 species has almost vanished, while the Q^3 resonance and, to a larger extend, the

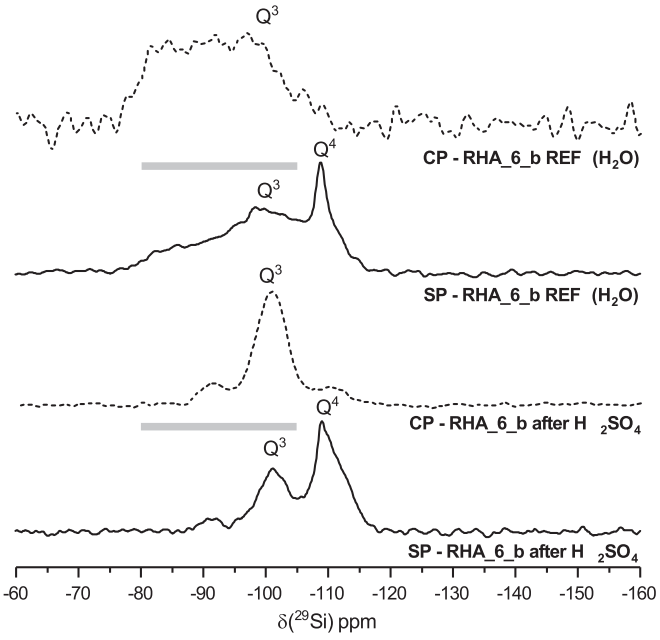

Fig. 8. ^{29}Si MAS NMR single-pulse spectra (denoted SP; full lines) and ^{1}H-^{29}Si CPMAS NMR spectra (denoted CP; dashed lines) of paste RHA_6_b after 70-day water-immersion and after 70-day exposure to sulfuric acid (pH = 1). The gray bar in the SP spectra marks the chemical shift range of Q^4(mAl) species with m = 1…4.

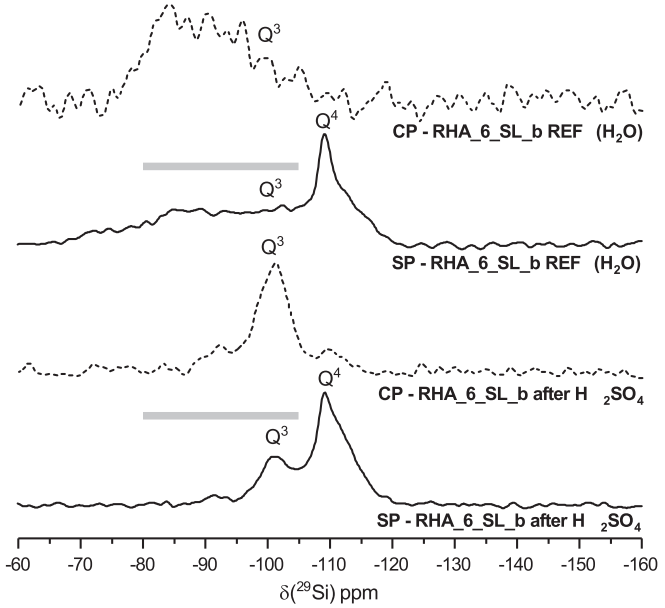

Fig. 9. ^{29}Si MAS NMR single-pulse spectra (denoted SP; full lines) and ^{1}H-^{29}Si CPMAS NMR spectra (denoted CP; dashed lines) of paste RHA_6_SL_ b after 70-day water-immersion and after 70-day exposure to sulfuric acid (pH = 1). The gray bar in the SP spectra marks the chemical shift range of $Q^4(m\text{Al})$ species with m = 1…4.

resonances of the geopolymeric gel are enhanced. Identical observations have been made previously for an as-cured, CR-based one-part AAM [29]. These results confirm that the Q^4 species in the unreacted RHA have no water in close proximity, while the Q^3 species in its leached surface layer are hydrated; the water in the pores of the geopolymeric gel [41] lead to an even more pronounced enhancement of the corresponding resonances in the CPMAS spectrum. In summary, RHA_6_b contained unreacted RHA, including cristobalite and a hydrated surface layer, and geopolymeric gel with a molar SiO_2/Al_2O_3 ratio in the range of approx. 3.5 to 4.

Fig. 9 (top two spectra) shows the ^{29}Si MAS NMR single-pulse and the ^{1}H-^{29}Si CPMAS NMR spectra of RHA_6_SL_b after water-immersion. Similar features as for the GGBFS-free RHA-based paste are present and can be interpreted in the same way, i.e. cristobalite at −109 ppm on top of a broad resonance from unreacted amorphous silica, the hydrated surface layer of the unreacted silica around approx. –99 ppm, and geopolymeric gel with $SiO_2/Al_2O_3 \approx 3.5$ extending downfield from near −99 ppm. However, the latter broad feature had a higher intensity compared to the Q^3 resonance, and it extends to more positive chemical shifts (up to approx. −70 ppm) than in the spectrum of RHA_6_b. The first characteristic indicates a higher degree of reaction of the RHA, which parallels the observations made on the MS-based pastes, where the addition of GGBFS increased the degree of reaction of the silica starting material too. The second characteristic can be interpreted in two ways: Either RHA_6_SL_b contained unreacted GGBFS (Q^0 species centered at −74 ppm [34]), or some C-A-S-H had formed in the paste (Q^1 centered around −79 ppm, as well as Q^2, Q^2(1Al) and Q^3(1Al) upfield [32–34]). The second explanation appears to be more likely, as GGBFS is known to be highly reactive in alkali-activated systems. The CPMAS spectrum of the water-immersed RHA_6_SL_b exhibits only a minor or no signal around −110 ppm from the cristobalite and the unreacted amorphous RHA-fraction, which have no water in close proximity. The lower intensity of the Q^3 resonance around −99 ppm, compared to the resonance of the geopolymeric gel in the CP spectrum, is in line with these intensities being rather similar in the single-pulse spectrum and a stronger enhancement for the water-rich gel.

The ^{29}Si MAS NMR and ^{1}H-^{29}Si CPMAS NMR spectra of RHA_6_b after acid exposure (Fig. 8, bottom two spectra) and RHA_6_SL_b after acid exposure (Fig. 9, bottom two spectra) can be discussed together. In both cases, the single-pulse spectra exhibit two prominent features at −110 ppm and −100 ppm, similar to what was observed for MS_6 and MS_6_SL after acid exposure (Fig. 7). In the spectra of the RHA-based materials, and additional minor resonance at approx. −92 ppm can be distinguished, and the resonance at −109 ppm has a rather narrow 'tip' on top. The two resonances at −110 ppm and −100 ppm are attributed to Q^4 (water-poor core) and Q^3 species (leached, hydrated surface layer) of silica phase(s), respectively, with the narrower peak on top of the Q^4 resonance related to cristobalite. These results show that the geopolymeric gel (and C-A-S-H, if present) had largely dissolved during the acid attack, leaving silica phase(s) that remained and/or were newly formed. The minor feature around −92 ppm is tentatively assigned to silicate species in remnants of the geopolymeric gel, that have been altered but not fully dissolved during the acid attack, possibly Q^3(1Al).

As for MS_6, chemical analyses of the RHA-based pastes after 70-day sulfuric acid exposure proved that only small amounts of Al remained in the pastes (RHA_6_b: 77.34 wt% SiO_2, 0.53 wt% Al_2O_3, < 0.01 wt% CaO, 0.24 wt% Na_2O, 0.34 wt% SO_3, and 19.92 wt% LOI; RHA_6_SL_b: 65.84 wt% SiO_2, 2.38 wt% Al_2O_3, 6.03 wt% CaO, 0.37 wt% Na_2O, 6.70 wt% SO_3, and 16.62 wt% LOI), thus confirming the presence of only a minor fraction of silicate species with Si—O—Al bridges in the NMR spectra. The presence of slightly more Al in the acid-exposed RHA_6_SL_b was expected from the persistence of gibbsite and bayerite in this specimen (Fig. 6).

The CPMAS spectra of the RHA-based, acid-exposed specimens differ considerably from the CPMAS spectra of the water-immersed pastes: (1) As the geopolymer had dissolved, no signal in the corresponding chemical shift range is observed, except for the small feature around −92 ppm, attributed to incompletely dissolved remnants. (2) The resonance of the Q^4 species at −109 ppm did not vanish fully, but instead can still be distinguished. (3) The resonance of the Q^3 species around −100 ppm is very much enhanced, compared to the single-pulse spectra. These two latter features are characteristic of the ^{1}H-^{29}Si CPMAS NMR spectra of highly-hydrated silica, i.e. silica gel with small particle sizes and correspondingly high surface area [42,43].

3.4. General discussion

The observations reported in the previous sections can be rationalized as follows: Dissolution of silicates in general [44], and zeolites in particular [45–47], occurs via (1) leaching of non-framework cations (alkali and/or alkaline earth ions), viz. substitution of Na^+ by H_3O^+ in the case of zeolite A, hydrosodalite and geopolymeric gel; followed by (2) removal of Al from the framework by hydrolysis of Si—O—Al bonds; and (3) eventually hydrolysis of Si—O—Si bonds, if such bonds are present in the structure. For zeolite A, step (2) already causes the complete destruction of the framework, since only Q^4(4Al) silicate species occur in the structure of zeolite A, i.e. each Si is bonded to four Al via Si—O—Al bonds [48]. Analogous reasoning is valid for hydrosodalite, which has $SiO_2/Al_2O_3 = 2$ too, and for geopolymeric gel with $SiO_2/Al_2O_3 \approx 2$, as in the CR-based and the MS-based one-part AAMs. However, the solubility of silica is low at neutral to acidic pH (2… 3×10^{-3} mol/dm^3 at pH < 8 for amorphous SiO_2 [49]), meaning that silica dissolved from the zeolites and the geopolymeric gel precipitates as silica gel at the acid/binder interface if the dissolved species are not washed away at a too high rate. This silica gel covers the surface of the exposed mortar and clogs pores, thereby inhibiting further dissolution, which explains the high acid resistance of the mortars based on MS-based geopolymer-zeolite composites. The silica gel is also responsible for the residual mechanical strength of the corroded layers of the mortars, and the fact that the paste samples without GGBFS addition did not disintegrate during the acid-exposure. In addition, because of its low solubility in acid, any unreacted silica (MS, RHA, or CR) in the

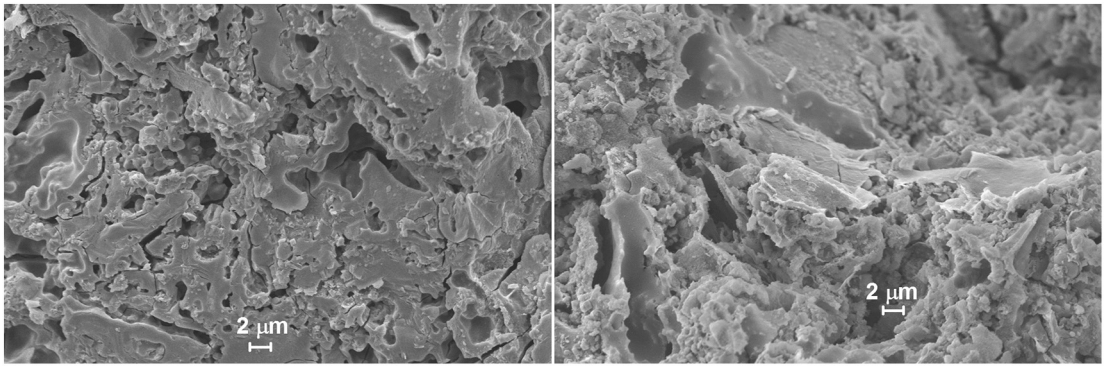

Fig. 10. SEM micrographs of fracture surfaces of paste RHA_6_b after 70-day water-immersion (left) and after 70-day exposure to sulfuric acid (pH = 1) (right).

materials will act as insoluble filler in the binder matrix, thereby improving the acid resistance of the mortars.

For the RHA-based geopolymers with a gel $SiO_2/Al_2O_3 \gg 2$, dissolution in acid may involve breaking of Si—O—Si bonds or may instead leave an Al-depleted silica framework, depending on the distribution of Si and Al in the framework (cf. Refs. [45, 46]). The fact that the effective depths of corrosion, $X_{f,D}$, as well as the visually observed corrosion depths were similar for analogous RHA-based and MS-based mortars as well as the similarity of the corresponding NMR spectra suggest that the same mechanisms are active in these materials, i.e. that at least part of silica of the RHA-based geopolymers is released into solution and subsequently precipitates as silica gel, providing protection to the surface. Support for the proposed mechanism is provided by SEM micrographs of paste RHA_6_b after 70-day water-immersion and after 70-day sulfuric acid exposure (Fig. 10). The water-immersed specimen exhibited a microstructure with 'glass-like' surfaces, representing the geopolymeric gel. On the contrary, the paste after acid-exposure exhibited 'debris-like', colloidal particles almost all over the surface, that are thought to be precipitated silica gel.

In previous studies of acid attack on low-Ca AAMs (geopolymers), the presence of silica gel after acid-exposure has been noticed too [12,13]. In these studies, the silica gel was interpreted only as a product of the deterioration of the geopolymeric gel, but it seemed not to have improved the microstructure of the materials; instead it was generally reported that the microstructures after acid attack were more porous than before the attack. The evidence obtained in the present work strongly suggests, however, that the precipitated silica gel provides mechanical strength to the corroded layer of the examined mortars, so that it remains in place and protects the inner regions of the mortars to some degree from acid attack.

In systems with the addition of GGBFS, i.e. binders with an increased Ca-content (MS_6_SL, RHA_6_SL_b), the same processes of dissolution and silica precipitation takes place, but in addition Ca^{2+} ions leached from the geopolymeric gel (or dissolved from C-A-S-H, if present) precipitate as gypsum, as has been observed by XRD (Figs. 3–6). Gypsum formation will generally lead to expansion and concomitant cracking, thereby allowing resumed ingress of the sulfuric acid and thus decreasing the acid resistance of the GGBFS-containing mortars compared to analogous mortars without GGBFS addition (Table 4).

4. Conclusions

Properly designed mortars, based on one-part alkali-activated binders made from silica and sodium aluminate, exhibit a sulfuric acid resistance that conforms to the requirements of DIN 19573:2016-03, Appendix A (70 days at pH = 1). This implies inter alia a sulfuric acid resistance sufficient for sewer network repair applications, where biogenic sulfuric acid attack is the major cause of degradation. Potentially, these mortars are also suitable for other applications where a high acid resistance is required, e.g. in agricultural structures; however, this needs to be verified by testing with organic acids. In the present study, a high acid resistance was achieved for mortars based on microsilica (MS) or rice husk ash (RHA) with a binder total molar SiO_2/Al_2O_3 ratio of 6, w/b ≤ 0.40, and a paste fraction of ~37 wt%. It is noted, that the temperature/RH conditions required for hardening of the mortars in sewer networks and similar structures can be created by passing hot water vapor into sections of the structure.

Exposure of the mortars to sulfuric acid leads to dissolution of the binder phases, viz. zeolite A and geopolymeric gel with $SiO_2/Al_2O_3 \approx 2$ in the case of the MS-based binders, and geopolymeric gel with SiO_2/Al_2O_3 around 3.5…4 in the case of the RHA-based binders, releasing sodium, aluminate and silica into solution. Due to the low solubility of silica at low pH, silica gel precipitates at the mortar/acid interface, inhibiting further degradation of the mortar. The silica gel imparts sufficient mechanical strength to the corroded mortar layer to prevent significant disintegration and loss of material, thus maintaining a transport barrier for the attacking sulfuric acid. In addition, unreacted silica particles in the binder matrix will act as insoluble filler, thereby improving its resistance.

As for mortars based on conventional cements (OPC, OPC/SCM blends, CAC), the acid resistance is not only influenced by the chemical composition of the binder, but also by the pore structure of the mortars, which in turn is determined by the particle size distribution of the mortar mix and by the w/b. This was demonstrated here by a mortar with w/b = 0.50 (CR_3.5), which had a comparatively low acid resistance. It can be concluded that for the silica gel precipitation to be protective, the w/b must be low enough to create a pore size distribution fine enough to allow the silica gel to block pores and protect the subjacent mortar.

Addition of GGBFS to increase the CaO content of the dry binders to 10 wt% (MS_6_SL, RHA_6_SL_b) leads to an increase of the degree of the reaction of the silica starting materials. At the same time, the sulfuric acid resistance of GGBFS-containing mortars was not conforming to the requirements of DIN 19573:2016-03, i.e. significantly lower than the resistance of the analogous mortars without GGBFS addition. This effect is caused by the formation of gypsum from released calcium and the sulfate ions of the acid solution, leading to expansion and associated crack formation, which facilitates ingress of the acid solution.

Acknowledgements

This work was supported by the German Federal Ministry for Economic Affairs and Energy and HERMES Technologie GmbH & Co. KG (Schwerte, Germany) via the program 'MNPQ-Transfer' (project No. 21/14). The authors a grateful to R. Hermes (HERMES Technologie) for valuable discussions, and to B. Mota (BAM) for support with the SEM analyses.

References

[1] W. Sand, E. Bock, Concrete corrosion in the Hamburg sewer system, Environ. Technol. Lett. 5 (1984) 517–528.
[2] M. Alexander, A. Bertron, N. De Belie (Eds.), Performance of Cement-based Materials in Aggressive Aqueous Environments: State-of-the-art Report, RILEM TC 211-PAE, Springer, 2013.
[3] J. Herisson, M. Guéguen-Minerbe, E.D. van Hullebusch, T. Chaussadent, Behaviour of different cementitious material formulations in sewer networks, Water Sci. Technol. 69 (2014) 1502–1508.
[4] C. Grengg, F. Mittermayr, G. Koraimann, F. Konrad, M. Szabó, A. Demeny, M. Dietzel, The decisive role of acidophilic bacteria in concrete sewer networks: a new model for fast progressing microbial concrete corrosion, Cem. Concr. Res. 101 (2017) 93–101.
[5] N. De Belie, J.J. Lenehan, C.R. Braam, B. Svennerstedt, M. Richardson, B. Sonck, Durability of building materials and components in the agricultural environment, part III: concrete structures, J. Agric. Eng. Res. 76 (2000) 3–16.
[6] A. Bertron, M. Peyre Lavigne, C. Patapy, B. Erable, Biodeterioration of concrete in agricultural, agro-food and biogas plants: state of the art and challenges, RILEM Tech. Lett. 2 (2017) 83–89.
[7] R. Hüttl, B. Hillemeier, Hochleistungsbeton – Beispiel Säureresistenz, Betonwerk + Fertigteil-Tech. 66 (1) (2000) 52–60 (in German).
[8] W. Breit, Säurewiderstand von Beton, in: G. Thielen (Ed.), Betontechnische Berichte 2001–2003, Verlag Bau + Technik, 2004, pp. 181–189 (in German).
[9] E. Gruyaert, P. Van den Heede, M. Maes, N. De Belie, Investigation of the influence of blast-furnace slag on the resistance of concrete against organic acid or sulphate attack by means of accelerated degradation tests, Cem. Concr. Res. 42 (2012) 173–185.
[10] A.M. Goyns, M.G. Alexander, Performance of various concretes in the Virginia experimental sewer over 20 years, in: C.H. Fentiman, R.J. Mangabhai, K.L. Scrivener (Eds.), Calcium Aluminates: Proceedings of the International Conference, Avignon, 18–21 May 2014, IHS BRE Press, 2014, pp. 573–584.
[11] J. Herisson, M. Guéguen-Minerbe, E.D. van Hullebusch, T. Chaussadent, Influence of the binder on the behaviour of mortars exposed to H_2S in sewer networks: a long term durability study, Mater. Struct. 50 (2017) 8.
[12] T. Bakharev, Resistance of geopolymer materials to acid attack, Cem. Concr. Res. 35 (2005) 658–670.
[13] A. Fernandez-Jimenez, I. García-Lodeiro, A. Palomo, Durability of alkali-activated fly ash cementitious materials, J. Mater. Sci. 42 (2007) 3055–3065.
[14] V. Sata, A. Sathonsaowaphak, P. Chindaprasirt, Resistance of lignite bottom ash geopolymer mortar to sulfate and sulfuric acid attack, Cem. Concr. Compos. 34 (2012) 700–708.
[15] C. Montes, E.N. Allouche, Evaluation of the potential of geopolymer mortar in the rehabilitation of buried infrastructure, Struct. Infrastruct. Eng. 8 (2012) 89–98.
[16] P.S. Deb, P.K. Sarker, S. Barbhuiya, Sorptivity and acid resistance of ambient-cured geopolymer mortars containing nano-silica, Cem. Concr. Compos. 72 (2016) 235–245.
[17] F.N. Okoye, S. Prakash, N.B. Singh, Durability of fly ash based geopolymer concrete in the presence of silica fume, J. Clean. Prod. 149 (2017) 1062–1067.
[18] A. Koenig, A. Herrmann, S. Overmann, F. Dehn, Resistance of alkali-activated binders to organic acid attack: assessment of evaluation criteria and damage mechanisms, Constr. Build. Mater. 151 (2017) 405–413.
[19] J. Temuujin, A. Minjigmaa, M. Lee, N. Chen-Tan, A. van Riessen, Characterisation of class F fly ash geopolymer pastes immersed in acid and alkaline solutions, Cem. Concr. Compos. 33 (2011) 1086–1091.
[20] R.R. Lloyd, J.L. Provis, J.S.J. van Deventer, Acid resistance of inorganic polymer binders. 1. Corrosion rate, Mater. Struct. 45 (2012) 1–14.
[21] J. Aliques-Granero, T.M. Tognonvi, A. Tagnit-Hamou, Durability test methods and their application to AAMs: case of sulfuric-acid resistance, Mater. Struct. 50 (2017) 36.
[22] A. Allahverdi, F. Škvára, Sulfuric acid attack on hardened paste of geopolymer cements: part 1. Mechanism of corrosion at relatively high concentrations, Ceramics-Silikáty 49 (2005) 225–229.
[23] A. Hajimohammadi, J.L. Provis, J.S.J. van Deventer, One-part geopolymer mixes from geothermal silica and sodium aluminate, Ind. Eng. Chem. Res. 47 (2008) 9396–9405.
[24] D. Feng, J.L. Provis, J.S.J. van Deventer, Thermal activation of albite for the synthesis of one-part mix geopolymers, J. Am. Ceram. Soc. 95 (2012) 565–572.
[25] G.J.G. Gluth, C. Lehmann, K. Rübner, H.-C. Kühne, Geopolymerization of a silica residue from waste treatment of chlorosilane production, Mater. Struct. 46 (2013) 1291–1298.
[26] T. Luukkonen, Z. Abdollahnejad, J. Yliniemi, P. Kinnunen, M. Illikainen, One-part alkali-activated materials: a review, Cem. Concr. Res. 103 (2018) 21–34.
[27] P. Sturm, S. Greiser, G.J.G. Gluth, C. Jäger, H.J.H. Brouwers, Degree of reaction and phase content of silica-based one-part geopolymers investigated using chemical and NMR spectroscopic methods, J. Mater. Sci. 50 (2015) 6768–6778.
[28] P. Sturm, G.J.G. Gluth, H.J.H. Brouwers, H.-C. Kühne, Synthesizing one-part geopolymers from rice husk ash, Constr. Build. Mater. 124 (2016) 961–966.
[29] S. Greiser, P. Sturm, G.J.G. Gluth, M. Hunger, C. Jäger, Differentiation of the solid-state NMR signals of gel, zeolite phases and water species in geopolymer-zeolite composites, Ceram. Int. 43 (2017) 2202–2208.
[30] Y. Shinohara, N. Kohyama, Quantitative analysis of tridymite and cristobalite crystallized in rice husk ash by heating, Ind. Health 42 (2004) 277–285.
[31] I. Ismail, S.A. Bernal, J.L. Provis, R. San Nicolas, S. Hamdan, J.S.J. van Deventer, Modification of phase evolution in alkali-activated blast furnace slag by the incorporation of fly ash, Cem. Concr. Compos. 45 (2014) 125–135.
[32] I.G. Richardson, A.R. Brough, R. Brydson, G.W. Groves, C.M. Dobson, Location of aluminium in substituted calcium silicate hydrate (C-S-H) gels as determined by ^{29}Si and ^{27}Al NMR and EELS, J. Am. Ceram. Soc. 76 (1993) 2285–2288.
[33] X. Pardal, F. Brunet, T. Charpentier, I. Pochard, A. Nonat, ^{27}Al and ^{29}Si solid-state NMR characterization of calcium-aluminosilicate-hydrate, Inorg. Chem. 51 (2012) 1827–1836.
[34] R.J. Myers, S.A. Bernal, R. San Nicolas, J.L. Provis, Generalized structural description of calcium–sodium aluminosilicate hydrate gels: the cross-linked substituted tobermorite model, Langmuir 29 (2013) 5294–5306.
[35] E. Lippmaa, M. Mägi, A. Samoson, G. Engelhardt, A.-R. Grimmer, Structural studies of silicates by solid-state high-resolution ^{29}Si NMR, J. Am. Chem. Soc. 102 (1980) 4889–4893.
[36] J.V. Smith, C.S. Blackwell, Nuclear magnetic resonance of silica polymorphs, Nature 303 (1983) 223–225.
[37] H. Rahier, B. van Mele, M. Biesemanns, J. Wastiels, X. Wu, Low-temperature synthesized aluminosilicate glasses. Part I. Low-temperature reaction stoichiometry and structure of a model compound, J. Mater. Sci. 31 (1996) 71–79.
[38] A. Palomo, S. Alonso, A. Fernandez-Jiménez, I. Sobrados, J. Sanz, Alkaline activation of fly ashes: NMR study of the reaction products, J. Am. Ceram. Soc. 87 (2004) 1141–1145.
[39] P. Duxson, J.L. Provis, G.C. Lukey, F. Separovic, J.S.J. van Deventer, ^{29}Si NMR study of structural ordering in aluminosilicate geopolymer gels, Langmuir 21 (2005) 3028–3036.
[40] R.A. Fletcher, K.J.D. MacKenzie, C.L. Nicholson, S. Shimada, The composition range of aluminosilicate geopolymers, J. Eur. Ceram. Soc. 25 (2005) 1471–1477.
[41] J.L. Provis, R.J. Myers, C.E. White, V. Rose, J.S.J. van Deventer, X-ray microtomography shows pore structure and tortuosity in alkali-activated binders, Cem. Concr. Res. 42 (2012) 855–864.
[42] G.E. Maciel, D.W. Sindorf, Silicon-29 nuclear magnetic resonance study of the surface of silica gel by cross polarization and magic-angle spinning, J. Am. Chem. Soc. 102 (1980) 7606–7607.
[43] I.S. Chuang, G.E. Maciel, A detailed model of local structure and silanol hydrogen bonding of silica gel surfaces, J. Phys. Chem. B 101 (1997) 3052–3064.
[44] E.H. Oelkers, General kinetic description of multioxide silicate mineral and glass dissolution, Geochim. Cosmochim. Acta 65 (2001) 3703–3719.
[45] R.L. Hartman, H.S. Fogler, Reaction kinetics and mechanisms of zeolite dissolution in hydrochloric acid, Ind. Eng. Chem. Res. 44 (2005) 7738–7745.
[46] R.L. Hartman, H.S. Fogler, Understanding the dissolution of zeolites, Langmuir 23 (2007) 5477–5484.
[47] H.L. Jamieson, H. Yin, A. Waller, A. Khosravi, M.L. Lind, Impact of acids on the structure and composition of Linde type A zeolites for use in reverse osmosis membranes for recovery of urine-containing wastewaters, Microporous Mesoporous Mater. 201 (2015) 50–60.
[48] C.A. Fyfe, J.M. Thomas, J. Klinowski, G.C. Gobbi, Magic-angle-spinning NMR (MAS-NMR) spectroscopy and the structure of zeolites, Angew. Chem. Int. Ed. Engl. 22 (1983) 259–275.
[49] J. Šefčík, A.V. McCormick, Thermochemistry of aqueous silicate solution precursors to ceramics, AIChE J. 43 (1997) 2773–2784.